International Journal of Aviation Science and Technology

Research Article

Passive Isolator Design and Vibration Damping of EO/IR Gimbal Used in UAVs

Mehmet Taha Görmüş[1], Bilal Faruk Adın[2], Paşa Yayla[3]*

[1] Marmara University, İstanbul/Turkey
mehmettaha6060@gmail.com - 0000-0001-7332-272X

[2] Marmara University, İstanbul/Turkey
adinbilalfaruk@gmail.com - 0000-0003-0378-523X

[3] Marmara University, İstanbul/Turkey
pasa.yayla@marmara.edu.tr - 0000-0002-1787-9475

Abstract

One of the most critical factors affecting the quality of the images captured by the surveillance systems used in the unmanned aerial vehicles is the vibrations transmitted from the aircraft to the gimbal. The gimbal used in unmanned aerial vehicles is essential equipment, holding the camera steadily and accurately and pointing it in the desired direction. Within the scope of this article, a passive vibration isolation system design has been made for the two-axis electro-optical gimbal used in the mini unmanned aerial vehicle. By choosing the spring-damper system among different methods, the design that isolates the harmonic vibration from the platform on a single axis has been made using the analytical method. The analytical method was used to create a design that isolates the harmonic vibration from the platform along a single axis. In addition, the part named 'Pan Yoke', which contains this damper system, was designed with a computer-aided design program, and natural frequency values were checked with Ansys modal analysis. The frequency of the vibration transmitted from the air vehicle to the gimbal and the natural frequency of the designed part have been determined to be close to each other, at around 200 Hz. The natural frequency values of this part were optimised with various design changes and topology optimisations to prevent the part from resonating.

Keywords

Passive vibration isolators,
Harmonic vibration,
Unmanned aerial vehicles,
Ansys modal analysis,
Topology optimisation

Time Scale of Article

Received 10 January 2023
Revised until 16 May 2023
Accepted 18 May 2023
Online date 28 June 2023

1. Introduction

The primary purpose of unmanned aerial vehicles is observation. Therefore, many proper loads, such as electro-optical (EO) and infrared (IR) cameras and synthetic aperture radar (SAR) systems, are being developed worldwide for this purpose. These systems cannot fully perform their duties when exposed to vibrations originating from the environment and unmanned aerial vehicles (UAV). Many different expressions are used for similar systems around the world, such as drones, UAV, unmanned aircraft systems (UAS), and remotely controlled aircraft systems. Instead of the term drone, UAV started being used in the 1990s. In the 2010s, since the UAV only refers to the flying platform and needs at least a control station and a data link in addition to the platform for flight, UAS have started to become widespread (Karaağaç, 2016).

Although there is no common understanding after the general nomenclature is made, these aircraft are generally classified according to their various characteristics (weight, altitude, etc.). In this article, since the design of an electro-optical payload is to be mounted on an unmanned aerial vehicle that will carry

*: Corresponding Author Paşa Yayla, pasa.yayla@marmara.edu.tr
DOI: 10.23890/IJAST.vm04is01.0104

approximately 10 kg of payload and reach an altitude of 2000 meters, this aircraft will be referred to as the "mini UAV" in the article. As a result, a vibration-damping device is built inside the gimbal, which holds the cameras on the UAV body. Vibration isolation or reduction using rubber pads, steel wire, or mechanical springs is "passive vibration isolation". The passive isolators exhibit some stiffness and damping, which are critical in constructing an effective isolator. The stiffness is used to calculate the isolator's corner frequency, which is often preferred when the isolator begins isolating vibration. When determining a system's absolute transmissibility, the corner frequency (ω) is essential. For disturbances at frequencies above $\sqrt{2}$ ω, the absolute transmissibility is less than one, and vibration isolation occurs spontaneously. When the disturbance frequency is less than $\sqrt{2}$ ω, vibration amplification occurs. Absolute transmissibility is unity for disturbance frequencies much lower than the corner frequency. The isolator performs best when the disturbance frequency is greater than $\sqrt{2}$ ω. The isolator's corner frequency should be kept as low as possible. However, reducing the corner frequency too much is impossible for various reasons. One of the reasons is the spring deflection value. For example, when the system is under static loading, the isolator must dampen vibration and support the static load (Sciulli, 1997).

Before the isolator design and gimbal modal analysis, this study surveyed the literature on UAV gimbal vibration damping systems. When looking at patents for the dates when imaging systems began to be stabilised using gimbals, the 1920s (Lucian, 1923) and 1930s (Richards, 1933) are seen as early examples. Since the 1960s, various patents have been obtained for products similar to today's gimbals, both in the fields of active control (Canlong and Zhimeng, 2022) and passive vibration isolation (Leavitt et al., 1972; Tyler, 1993; Kiunke, 1993; Norén and Segerström, 1998). As we approach today, we see a complex gimbal vibration isolator design in which coils spring, elastomer, and magnetic insulators are used together in a patent obtained in 2017 (Levis, 2017). Again in 2017, it is seen that coil springs and insulators are mentioned for a large and complex gimbal (Zeise and Anderson, 2017). Another patent related to the elastomer mentioned a damper produced by moulding rubber between metal plates used as a vibration isolator (Tian and Jian, 2019). Steel wire rope and viscous damper are also used as passive vibration isolators in UAVs, as seen in a sample patent (Zhang et al., 2020).

In light of these technological solutions, it is seen that vibration-damping systems are essential in many sectors. Some damping methods in the literature are examined, and the elements used in these designs, such as spring, damper, elastomer, ring, wire and electromagnetic magnet, are investigated.

For example, in automotive, it is seen that the combination of a spring coil and a viscous damper is used in the vehicle suspension system (Kumar, 2021) and the seat system (Tewari and Prasad, 1999) to reduce the vibration reaching the driver. Elastomeric dampers are generally used to prevent the transmission of vibration generated by the internal combustion engine to the vehicle (Bursa, 2019).

One of the methods used in vibration isolation is the material referred to as “wire rope” in the literature (Balaji et al., 2017; Weimin et al., 1997). A wire rope isolator is generally used for small action camera-like systems on the quadcopter.

This study aims to re-design a lighter and novel gimbal system's vibration isolation system for a small class UAV using a spring and damper to prevent pan yoke resonance.

2. Requirements for the Design and the Methodology

For the design of the isolator, the characteristics of the vibration to which the system will be exposed should be known. Vibration data can be obtained from guidelines prepared for vibrations under various conditions (MIL-STD-810) or vibration sensors. Vibration analysis begins by plotting amplitude versus time. This is called time-domain data. These data are obtained from the various sensors. Usually, such data do not yield meaningful results, and converting them to the frequency domain is necessary.

For this article, data could be collected with accelerometers placed on a mini UAV. Thus, all random and harmonic vibration values can be obtained for that UAV. However, due to the lack of technical equipment, a general literature study was preferred to define the main vibration source for mini UAVs.

The vibration source in the aircraft can be classified into three main groups: vibrations originating from the external environment, vibrations from the propulsion system of the aircraft, and vibrations arising from other functions of the aircraft. Vibrations originating from the external environment are ground vibrations during taxi and take-off (Burström et al., 2006) and vibrations caused by aerodynamic forces during flight (Liu, 2020).

This study considers the engine as the primary vibration source in mini-UAVs. According to the design criteria obtained by examining these studies, first, the spring stiffness value and damping coefficient are calculated analytically, and then the spring design is made with these values. Then, after the spring and damper systems are designed, the pan yoke design is accomplished, the mode shapes are examined, and design changes are

made so that the gimbal does not resonate.

Since the gimbal designed within the scope of this work does not take images during the UAV's taxi, take-off, and landing phases, only the cruise phase is taken into account during the modelling of the vibration to which the optical system is exposed. During the cruise, vibrations caused by aerodynamic forces and the vibration of the UAV engine are effective. Turbulence, which an aircraft is subjected to, can be used as an example of an aerodynamic force. The damping rate of this vibration of the passenger seats is investigated in the work of Ciloglu and his co-authors on the magnitude of these vibrations at different flight stages (Ciloglu et al., 2015). However, since modelling the vibration caused by aerodynamic forces would be so comprehensive that it would be another topic, only engine-induced vibrations are examined in this article.

In the work by Lai and Jan (Lai and Jan, 2011), the effect of the engine vibration of the mini UAV on the GPS was investigated. The UAV mentioned in this work has an 80 cc two-stroke gasoline engine with a 3.5 m wingspan. Ge and his co-workers (Ge et al., 2021) found that the UAV's in-flight vibration intensities at the horizontal level were consistently higher than those in the vertical direction.

Also, according to Lai and Jan (Lai and Jan, 2011), temporal information is lost in the conversion process. However, in their study, the vibration frequency changed over time as the aircraft was operated under different flight conditions. Because of this, the short-time-Fourier transform method was used to observe the temporal information in the frequency domain, and the dominant vibration frequency at different times during the flight was determined. If the determined frequencies are examined, it can be seen that they are related to the engine speed and propeller speed and are between 100-150 Hz during the cruise.

Since the multi-rotor aircraft used in a recent work (Ge et al., 2021) and other similar studies have electric motors and many propellers, they may not show the same vibration characteristics as the piston engine and single propeller mini unmanned aerial vehicles that are the subject of this article.

The design requirements of the targeted gimbal are given in Tables 1 and 2.

Table 1. Design requirement and its physical properties

Necessary Properties	Numerical Value
Dimensions	H250 mm, W230 mm, L230 mm
Optical System Weight	1.5 kg
Gimbal Weight	< 5 kg
Yaw Angle	360°
Pitch Angle	-30°, +110°

$$Frequency\ of\ Engine = \frac{12000\ rpm}{60} = 200\ Hz$$

Table 2. Design requirement and its vibration characteristics

Characteristics of Excitation Vibration	Type and Limitation
Vibration Type	Harmonic Base Excitation
Excitation Frequency	200 Hz
Required Isolation	97%
Max Static Deflection	0.3 mm

3.Calculations

3.1. Isolation System Design Calculations

The transmissibility plot and iterations may be needed to select the correct k_{eq} and c_{eq} values for the targeted design. First, some necessary parameters can be used to understand the transmissibility graph Figure 1, and create the iteration table, Table 1.

$$\omega_n = \sqrt{\frac{k}{m}} \quad (1)$$

$$r = \frac{\omega}{\omega_n} \quad (2)$$

$$\zeta = \frac{c}{2\sqrt{km}} \quad (3)$$

After that, using the transmissibility ratio, the ratio of output to input, the right k and c values can be easily chosen.

$$\beta = \sqrt{\frac{1+(2*\zeta*r)^2}{(1-r^2)^2+(2*\zeta*r)^2}} \quad (4)$$

Moreover, static deflection can also be considered for choosing k_{eq} and c_{eq} values;

$$\delta = \frac{mg}{k} \quad (5)$$

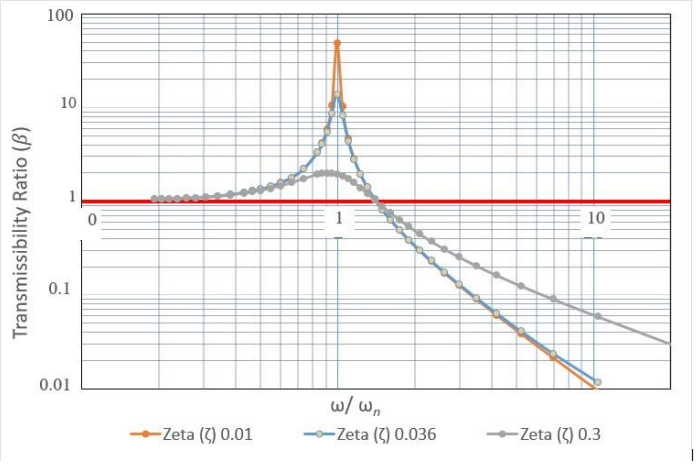

Fig. 1. Transmissibility of gimbal structural system

Firstly, the iteration can be started with m = 1.5 kg (defined earlier in the system requirements) and k_{eq} =

1000 N/m, and c_{eq} = 2 Ns/m. The iterations were executed using Excel and are listed in Table 3. The iteration was started with small k_{eq} and c_{eq} values because if it is started with large values, it may miss intermediate values smaller than the initial value. It is also seen in Figure 1 that the 0.03 transmissibility ratio for different zeta (ζ) values in Table 3 is obtained around the r-value of approximately 7.x

Figure 1 illustrates how the transmissibility value significantly rises as the r value gets closer to 1. The circumstance is known as resonance. This demonstrates that no vibration damping is used in the design and that the vibration is conveyed without damping. Different k_{eq} and c_{eq} values are introduced into the equations to produce better transmissibility and deflection values in order to avoid this problem.

The dumping coefficient employed in the system is determined using the damping ratio designated as zeta in the formulas and diagrams. Transmissibility is influenced by three elements, as shown in Figure 1. These are the system's dumping ratio, the driving frequency, and the part's inherent frequency. The (r) value must be as high as feasible for the low transmissibility to occur. On the other hand, the drive frequency is a value that operates outside and cannot be altered. Because the system's stiffness cannot be decreased below the level necessary for static strength, the natural frequency cannot be reduced to extremely low values.

Even at equal driving and natural frequencies, resonance is avoided by the large damping ratio. For values when the zeta is high, increasing the (r) value is insufficient to achieve the necessary transmissibility value. The transmissibility values derived for various damping ratios and (r) values are displayed in Figure 1 and Table 3.

Table 3. Iteration to find k_{eq} and c_{eq} values for the system

Iteration Number	k_{eq} (N/m)	c_{eq} (Ns/m)	ζ	r	β	δ (mm)
1	1000	2	0.02582	48.67	0.00114	14.715
2	10000	2	0.00817	15.39	0.00437	1.4715
3	20000	5	0.01443	10.88	0.00893	0.7358
4	30000	8	0.01886	8.89	0.01353	0.4905
5	40000	15	0.03062	7.70	0.01899	0.3679
6	50000	20	0.03652	6.88	0.02413	0.2943

The iteration can be stopped after the sixth iteration because static deflection and transmissibility values are acceptable for system requirements.

k_{eq} value is 50000 N/m and c_{eq} value is 20 Ns/m (6)

Analytical calculation of natural frequency:

$$\omega_n = \sqrt{\frac{50000}{1.5}} = 182.57 \frac{rad}{s} = 29.05Hz \quad (7)$$

3.2. Analytical Solution of Equation of Motion

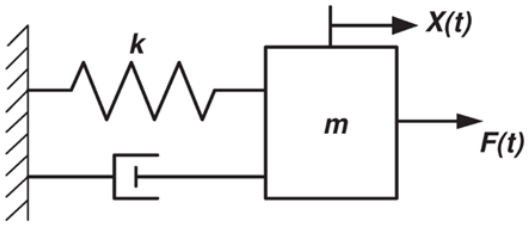

Fig. 2. A Mass- spring- damper system with external force

$$m_{eq}\ddot{x} + c_{eq}\dot{x} + k_{eq}x = F_{eq}(t) \quad (8)$$

The general solution can be written using Equation 9;

$$x(t) = x_h(t) + x_p(t) \quad (9)$$

After some requirements and iterations (k_{eq} and c_{eq}) value of these physical properties can be listed below:

$$m_{eq} = 1.5\ kg$$
$$c_{eq} = 20\ Ns/m$$
$$k_{eq} = 50000\ N/m \quad (10)$$
$$F_{eq} = 500 \sin(942.48t)\ N$$

After determining the values of properties, the homogenous solution can be solved first.

$$1.5\ \ddot{x} + 20\ \dot{x} + 50000\ x = 0 \quad (11)$$

The characteristic equation becomes:

$$1.5\ r^2 + 20\ r + 50000 = 0 \quad (12)$$

Roots can be found as follows:

$$r_{1,2} = -\frac{20}{3} \pm i\ \frac{20\sqrt{749}}{3} \quad (13)$$

Hence, the homogenous solution can be found using differential equation knowledge:

$$x_h(t) = e^{\left(-\frac{20}{3}\right)t}\left(C_1 \cos\left(\frac{20\sqrt{749}}{3}t\right) + C_2 \sin\left(\frac{20\sqrt{749}}{3}t\right)\right) \quad (14)$$

$$x_h(t) = e^{\left(-\frac{20}{3}\right)t}\left(C_1 \cos(182.452t) + C_2 \sin(182.452t)\right) \quad (15)$$

Then, the particular solution can be determined using the method of undetermined coefficients method:

$$x_p(t) = A cos(942.48t) + B sin(942.48t) \quad (16)$$

The first and second derivatives of a particular solution can be found as:

$$\dot{x_p}(t) = (-942.48)\ A\ sin(942.48t) + (942.48)\ B\ cos(942.48t) \quad (17)$$

$$\ddot{x_p}(t) = -(942.48)^2\ A\ cos(942.48t) - (942.48)^2\ B\ sin(942.48t) \quad (18)$$

The first and second derivatives can be put into the

damper-spring-mass (Figure 2) differential equation:

$$1.5\left(-(942.48)^2\ A\ cos(942.48t) - (942.48)^2\ B\ sin(942.48t)\right) + 20\left((-942.48)\ A\ sin(942.48t) + (942.48)\ B\ cos(942.48t)\right) + 50000\ (Acos(942.48t) + Bsin(942.48t)) = 500\sin(942.48t) \quad (19)$$

$cos(942.48t)$ and $sin(942.48t)$ terms are gathered separately:

$$cos(942.48t)(-1.5(942.48)^2\ A + 20\ ((942.48)\ B + 50000\ A) = 0 \quad (20)$$

Roots can be found as follows:

$$sin(942.48t)(-1.5(942.48)^2\ B - 20\ \left((942.48)\ A + 50000\ B\right) = 500\ sin(942.48t) \quad (21)$$

Then the A and B coefficients can be found as:

$$A = -5.73\ x10^{-6}\ \&\ B = -\ 3.90\ x10^{-4} \quad (22)$$

After that, the particular solution can be found as follows:

$$x_p(t) = -5.73x10^{-6}cos(942.48t) - 3.90\ x10^{-4}\ sin(942.48t) \quad (23)$$

The general solution can be written as follows:

$$x(t) = e^{\left(-\frac{20}{3}\right)t}\ (3.06x10^{-4}\cos(182.452t) + 0.00202\sin(182.452t)) - 5.73x10^{-6}cos(942.48t) - 3.90\ x10^{-4}\ sin(942.48t \quad (24)$$

Equation 24 can be plotted in Matlab by choosing t=0:0.01:2, as shown in Figure 3.

Figure 3 illustrates the displacement motion of the nonhomogeneous mass-spring-damper system against time. It shows the characteristic behaviour of the vibration against time and how long the vibration is damped.

4.Numerical Analysis

A bracket was designed to hold the motor connected to the shaft and springs, whose stiffness values were calculated analytically and placed between the bracket and the yoke. In addition, since the system is modelled as 1 DOF in the analytical solution, the constraints to ensure this have been considered in the design.

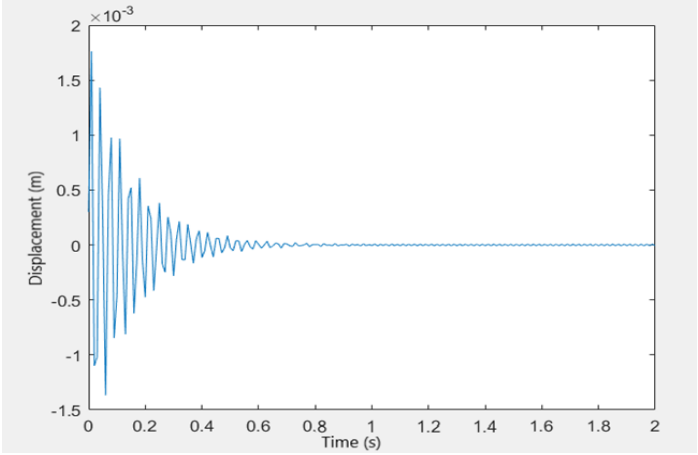

Fig. 3. Hand solution of forced vibration equation, Equation 24

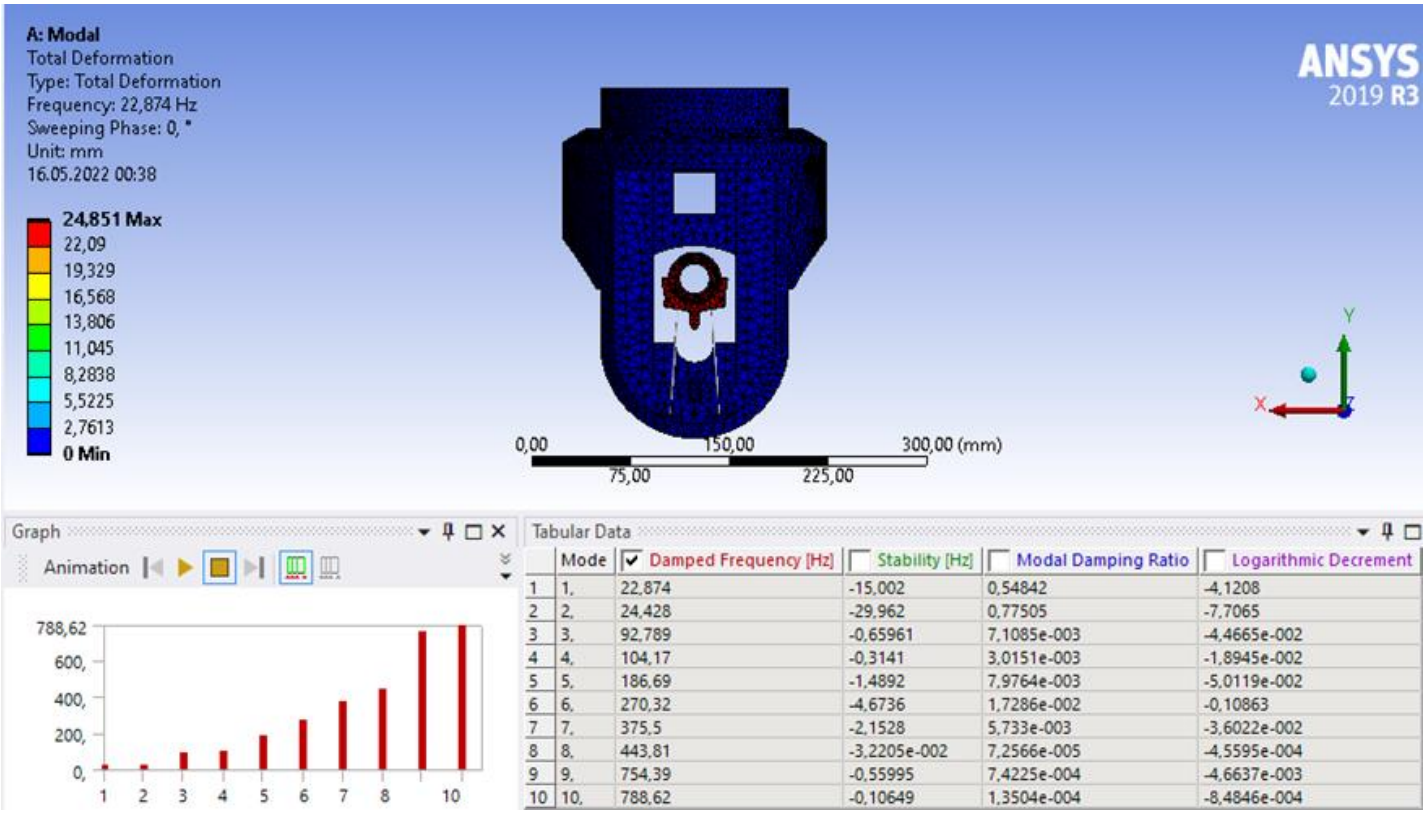

	Mode	Damped Frequency [Hz]	Stability [Hz]	Modal Damping Ratio	Logarithmic Decrement
1	1.	22,874	-15,002	0,54842	-4,1208
2	2.	24,428	-29,962	0,77505	-7,7065
3	3.	92,789	-0,65961	7,1085e-003	-4,4665e-002
4	4.	104,17	-0,3141	3,0151e-003	-1,8945e-002
5	5.	186,69	-1,4892	7,9764e-003	-5,0119e-002
6	6.	270,32	-4,6736	1,7286e-002	-0,10863
7	7.	375,5	-2,1528	5,733e-003	-3,6022e-002
8	8.	443,81	-3,2205e-002	7,2566e-005	-4,5595e-004
9	9.	754,39	-0,55995	7,4225e-004	-4,6637e-003
10	10.	788,62	-0,10649	1,3504e-004	-8,4846e-004

Fig. 4. Modal analysis results of first gimbal

The natural frequency, calculated analytically as 29.05 Hz, was found to be 22.87 Hz in Ansys (1st mode longitudinal axis of spring), as shown in Figure 4. One of the reasons for this was that the weight assumed in the analytical solution was 1.5 kilograms due to the weight of the optic ball. However, during the analysis, the motor that moves the optical system and the weight of the brackets holding these motors are added to the system. When the weight of the motors and brackets, approximately 400 grams, is considered in the analytical solution, the natural frequency is obtained as 25.81 Hz.

Sweeping phase 0 refers to the first step of the analysis, where the software calculates the static deformation of the structure due to the loads applied to it. This is also known as the "pre-stress" or "pre-load" step. During this phase, the software applies the loads to the structure and calculates the corresponding displacements and deformations. The results of this step are then used as the initial conditions for the dynamic analysis that follows.

The modal damping ratio is expressed as the ratio of the actual damping in a mode to the critical damping for that mode. Critical damping corresponds to the minimum amount of damping required for a system to return to its equilibrium position before oscillating after a disturbance. The ratio decreased in every mode.

After the static analysis, the result shown in Figure 5(a) was obtained using the Ansys topology module. Here, the objective function was chosen for topology optimisation to minimize compliance and maximize the natural frequency. Considering this result and the part's manufacturability, Figure 5(b) was designed with SolidWorks. Following this stage, the yoke's modal analysis was repeated several times, and design changes were made to increase the lowest natural frequency without significantly increasing the mass, Figure 5(c).

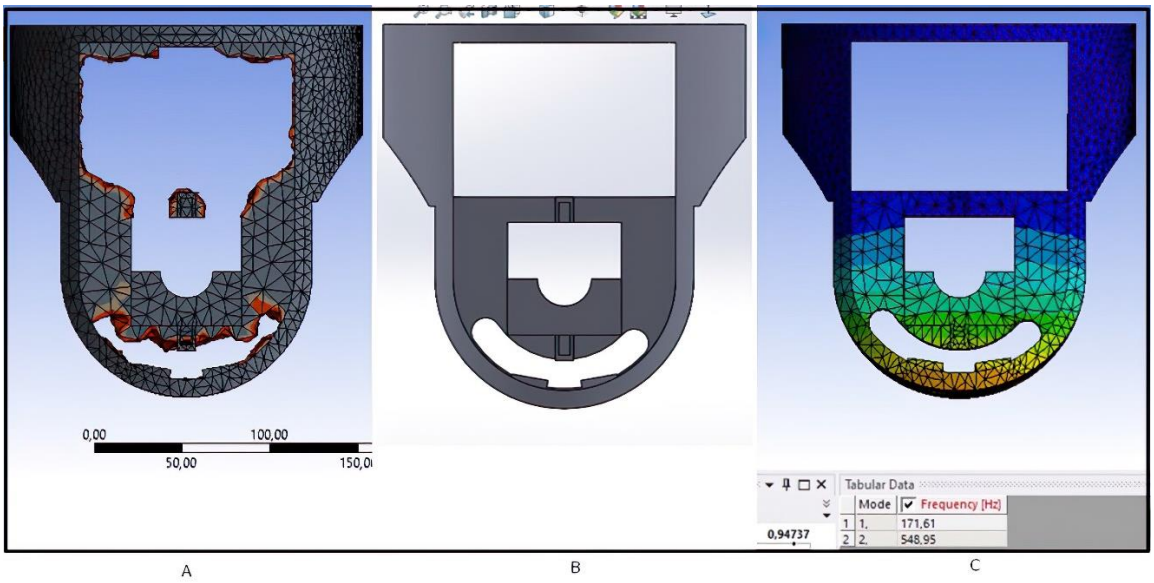

Fig. 5. Topology optimisation result (A), CAD design (B), modal analysis (C)

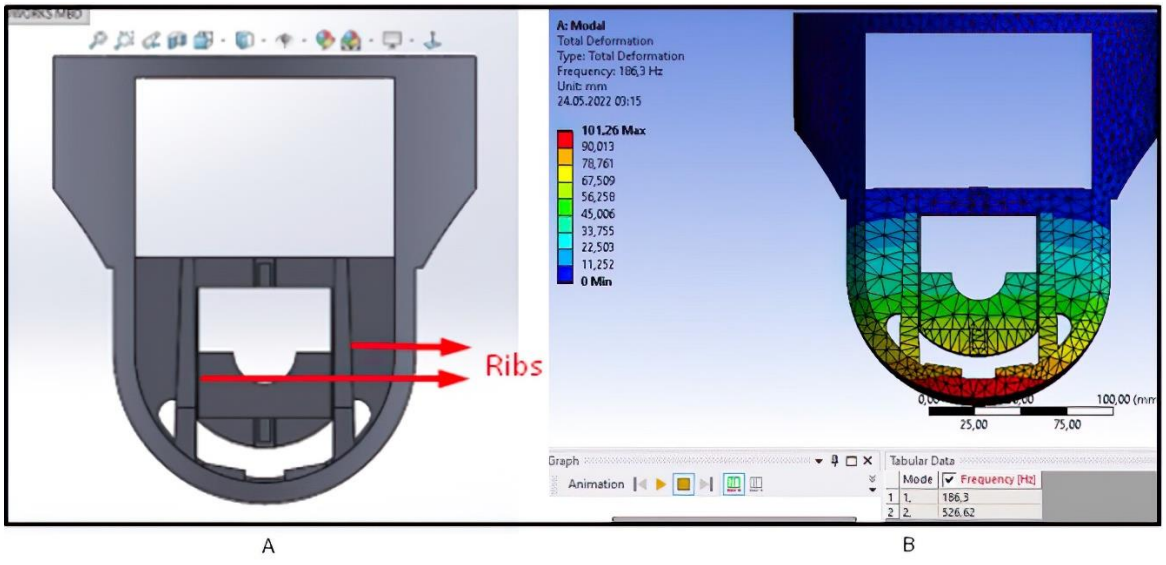

Fig. 6. CAD design with ribs (A) and its modal analysis (B)

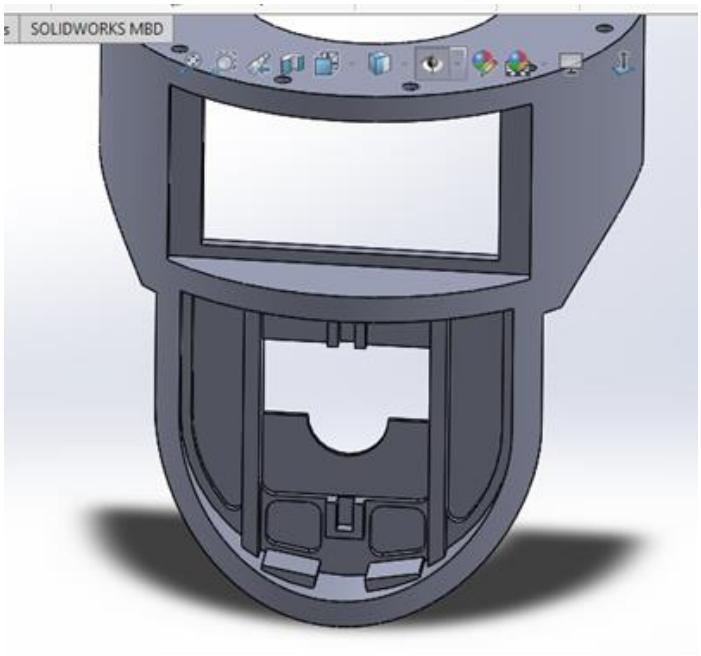

Fig. 7. Mid-section thickened design

Table 4. Effect of the mesh size on the natural frequencies

Mode	Mesh Size 7 mm Frequency (Hz)	Mesh Size 6 mm Frequency (Hz)	Mesh Size 5 mm Frequency (Hz)
1	22.673	22.673	22.673
2	24.649	24.649	24.65
3	388.24	385.91	383.35
4	474.11	472.03	468.34
5	474.12	472.14	470.49
6	540.6	538.43	535.83

After the design changes in Figures 6 and 7 were made, the final design seen in Figure 8 was obtained.

For the analysis mentioned in the design part, an average mesh size was chosen for rapid analysis. In this part of the work, the final design was analysed to see how the obtained results related to mesh quality and size. If the changes in the natural frequencies obtained by changing the mesh are small, it can be assumed that the natural frequency values will converge to a certain value.

After reaching the final design mesh size, the analysis can be executed. To accomplish this, three different mesh sizes are chosen. These mesh sizes are 7 mm, 6 mm, and 5 mm. The natural frequency values of the final design obtained with these different meshes are shown in Table 4 and Figures 9-11.

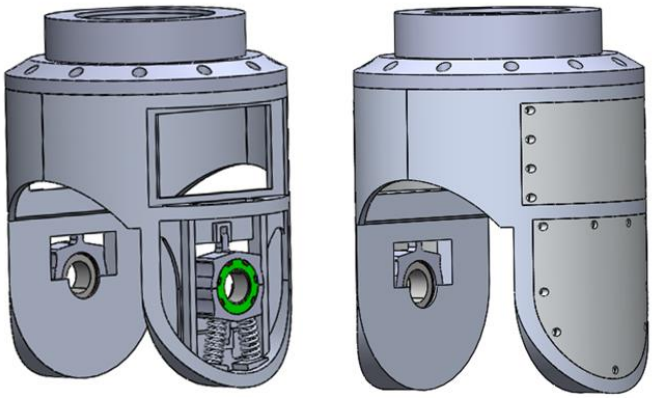

Fig. 8. Final gimbal design without cover and with cover

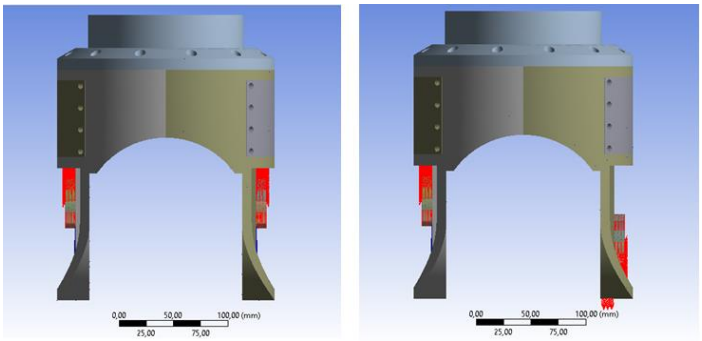

Fig. 9. First mode shape 22.673 Hz (left) and the second mode shape 24.65 Hz (right)

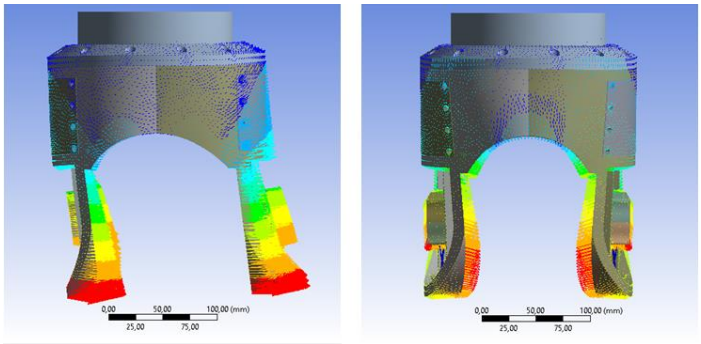

Fig. 10. Third mode shape 383.35 Hz (left) and the fourth mode shape 468.34 Hz (right)

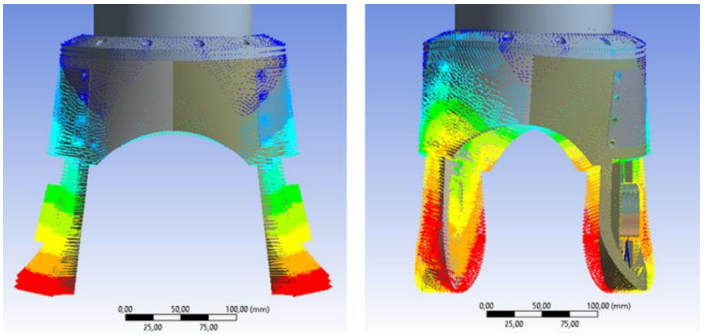

Fig. 11. Fifth mode shape 470.49 Hz (left) and the sixth mode shape 535.83 Hz (right)

5. Results and Discussions

In this study, an ideal design of a passive isolation system is obtained for the EO/IR gimbal used in mini unmanned

aerial vehicles by using the spring and damper, which are the essential mechanical isolation elements. While making this design, an iterative method is followed by using the necessary formulations for spring constant and damping coefficient selection. Then, to see the vibration damping after the k and c values were found by the iterative method, the quadratic non-homogeneous differential equation was solved by hand and plotted with Matlab.

The spring stiffness was calculated as 50000 N/m and the damping coefficient as 20 Ns/m in the design, which gave a 3% transmissibility rate for 97% vibration isolation in the design requirements.

Then the part weight is minimised with topology optimisation. After the topology optimisation, the mass was reduced by approximately 15%.

After topology optimisations, the final part design was subjected to modal analysis. Initially, the system's natural frequencies coincided with the base excitation frequency and entered a state of resonance. To prevent this, some changes in the design of our piece were made. For example, adding a rib moved the natural frequency values away from the base excitation frequency value.

- The third natural frequency increased from 92.8 Hz to 388.4 Hz.
- The fourth natural frequency increased from 104.2 Hz to 468.3 Hz.
- The fifth natural frequency increased from 186.7 Hz to 470.5 Hz.

After reaching the desired natural frequency values, the analysis was performed in 3 different mesh sizes (5 mm, 6 mm, and 7 mm) to observe the effect of mesh size on the results.

- A difference of less than 1% was observed in the frequency results obtained when the mesh number was increased.

6. Conclusions

This study presents a lighter and novel passive isolator system and gimbal design, considering the vibration that the gimbal in a mini unmanned aerial vehicle is exposed to and validated with modal analysis. It is revealed where the vibration originates, how it can be dampened, and how the design can be altered to prevent resonance in the system.

With this study, a novel design of a passive isolation system is obtained. Following topological optimization, the mass of the passive isolator was decreased by 15% or such.

In future studies, more realistic results can be obtained from the harmonic vibration assumption considered in the current work by experimentally performing vibration measurement and spectrogram analysis on the UAV. Afterwards, the analyses were made with a CAD design in which all optics and electronic parts, even nuts and gaskets, are modelled in the gimbal and can be more helpful in determining the natural frequencies and mode shapes. Finally, as it may yield more realistic results, choosing a system with multiple degrees of freedom rather than a single one is possible.

Acknowledgement

The authors would like to thank TÜBİTAK for supporting the work within the scope of the 2209-A University Students Research Projects Support Program, which provides financial support. The technical support provided by Blitz Systems is also well appreciated.

CRediT Author Statement

Mehmet Taha Görmüş: Investigation, Conceptualization, Methodology, Analysis, Original draft preparation. **Bilal Faruk Adın**: Investigation, Conceptualization, Methodology, Analysis, Data curation, Writing- Original draft preparation. **Paşa Yayla**: Supervision, Investigation, Conceptualization, Methodology, Writing- Reviewing and editing.

References

Balaji, P. S., Moussa, L., Khandoker, N., Shyh, T. Y., Rahman, M. E. and Ho, L. H. (2017) 'Experimental study on vertical static stiffnesses of polycal wire rope isolators', In IOP Conference Series, Materials Science and Engineering, 217(1): p. 012032), IOP Publishing. doi:10.1088/1757-899X/217/1/012032

Bursa, A.İ. (2019) 'Vibration Transmission Investigation of Engine Mounting Brackets', MSc Thesis, İTÜ, Institute of Science and Technology, Istanbul-Turkey, (In Turkish).

Burström, L., Lindberg, L., and Lindgren, T. (2006). Cabin attendants' exposure to vibration and shocks during landing. Journal of Sound and Vibration, 298(3), 601-605. https://doi.org/10.1016/j.jsv.2006.06.026

Canlong, L. and Zhimeng, S. (2022) 'Control methods, apparatus, and device, and UAV', United States, Patent No. US11216013B2, (2022).

Ciloglu, H., Alziadeh, M., Mohany, A. and Kishawy, H. (2015) 'Assessment of the whole body vibration exposure and the dynamic seat comfort in passenger aircraft', International Journal of Industrial Ergonomics, 45, pp. 116-123. doi:10.1016/j.ergon.2014.12.011

Ge, C., Dunno, K., Singh, M. A., Yuan, L., and Lu, L. X.

(2021). Development of a drone's vibration, shock, and atmospheric profiles, Applied Sciences, 11(11), 5176. doi:10.3390/app11115176

Karaağaç, C. (2016). İHA Sistemleri Yol Haritası Geleceğin Hava Kuvvetleri 2016-2050. STM-Mühendislik Teknolojik Danışmanlık, retrieved from https://thinktech.stm.com.tr/uploads/docs/1608914423_satm-bb-17-0200-sektor-raporlari-iha-260417.pdf

Kiunke, P.C. and Schaefer, R. D. (1993) 'Gimbal vibration isolation system', European Patent Office, Patent No. EP0559402A2, (1993).

Kumar, D. (2021) 'Durability analysis of helical coil spring in vehicle suspension systems', PhD Thesis, Virginia Tech., USA.

Lai, Y. C. and Jan, S. S. (2011) 'Attitude estimation based on fusion of gyroscopes and single antenna GPS for small UAVs under the influence of vibration', GPS Solutions, 15(1), pp. 67-77. doi:10.1007/s10291-010-0171-y

Leavitt, J.N., Alas, R. and Dafoe, E.C. (1972) 'Stabilized camera mount' United States, Patent No. US3638502.

Levis, M.D. (2017) 'Platform stabilisation system', United States, Patent No. US9765925B2.

Levis, M.D. (2001) 'Stabilized platform systems for payloads', United States, Patent No. US6263160.

Liu, Y. (2020). Study on the vibrational comfort of aircraft in formation flight. Aircraft Engineering and Aerospace Technology, 92(8), 1307-1316. doi.org/10.1108/AEAT-12-2018-0311

Lucian, A.N. (1923) 'Stabilizer', United States, Patent No. US1634950.

Norén, K. and Segerström, T. (1998) 'A Device for stabilizing of a remotely controlled sensor, like a camera', European Patent Office, No: WO1998016871A1.

Richards, W.H. (1933) 'Universal camera mount', United States, Patent No. US1955770.

Sciulli, D. (1997) 'Dynamics and Control for Vibration Isolation Design' PhD Thesis, Virginia Polytechnic Institute and State University, USA.

Tewari, V. K. and Prasad, N. (1999) 'Three-DOF modelling of tractor seat-operator system", Journal of Terramechanics, 36(4), pp. 207-219. doi:10.1016/S0022-4898(99)00008-7

Tian, Y. and Jian, W. (2019) 'Gimbal vibration damper for UAVS', United States, Patent No. US10260591B2.

Tyler, N. (1993) 'Gyroscopically stabilized apparatus', United States, Patent No. US5184521A.

Weimin, C., Gang, L. and Wei, C. (1997) 'Research on ring structure wire-rope isolators', Journal of Materials Processing Technology, 72(1); pp. 24-27. doi:10.1016/S0924-0136(97)00124-6

Zeise, S.W., and Anderson, R.D. (2017) 'Gimbal system having preloaded isolation', United States, Patent No. US2017175948A1.

Zhang, S., Zhang, Y. and Liang, G. (2020) 'Damping device, gimbal assembly having same, and unmanned aerial vehicle', United States, Patent No. US2020307826A1.